Journal of Materials Chemistry A

Accepted Manuscript

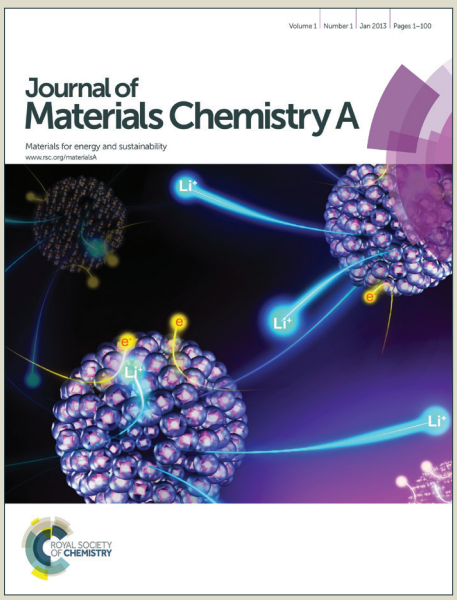

ROYAL SOCIETY OF CHEMISTRY

www.rsc.org/materialsA

Journal of

Materials Chemistry A

RSCPublishing

PAPER

One-step Synthesis of Mesoporous MnO_2/carbon Sphere Composites for Asymmetric Electrochemical Capacitors

Cite this: DOI: 10.1039/x0xx00000x

Guoxiang Wang,[ab] Hongfeng Xu,*[b] Lu Lu [b] and Hong Zhao[b]

Received 00th January 2014,
Accepted 00th January 2014

DOI: 10.1039/x0xx00000x

www.rsc.org/

Whisker-like MnO_2/carbon sphere (MnO_2/C) composites with a mesoporous structure are synthesized through an easy one-step hydrothermal method using glucose as carbon sources without any catalyst or template. Highly porous interconnected MnO_2 nanowhiskers are uniformly coated on the surface of the carbon sphere to construct a mesoporous architecture. A high-voltage asymmetric electrochemical capacitor (EC) is assembled with active carbon as the negative electrode and MnO_2/C spheres as the positive electrode in a neutral aqueous 5 M $LiNO_3$ solution as electrolyte. This aqueous electrolyte-based asymmetric EC is reversibly cycled within the wide-voltage region of 0-2.0 V. Moreover, a high specific capacitance of 307.6 F g^{-1} and a superior long-term cyclic stability of nearly 96.6% retention after 1000 cycles are observed.

Introduction

Supercapacitors, also as known as electrochemical capacitors or ultracapacitors, are attracting considerable interest because of their combined merits, i.e., high energy density of batteries and high power density of conventional dielectric capacitors.[1–5] Supercapacitors can be divided into two types based on energy storage mechanism, such as: electrical double-layer capacitors (EDLCs) that use carbon-active electrode materials and pseudocapacitors that employ metal oxides and conduct polymers electrode materials.[6–8] Each type of electrode material has specific advantages and disadvantages.[9–12] Carbon materials have high power density and long cycle life but low specific capacitance.[9,10] The metal oxides have higher energy density compared to conventional carbon materials and better cycling stability than polymer materials, however, they have lower energy density than lithium ion battery immensely, which limit their application.[11,12] The resolution of these problems inspires attempts in developing novel electrode materials by coupling carbon materials with high electrical conductivity and electrochemically active materials as electrode for the supercapacitor.

Manganese dioxides (MnO_2) is an attractive option among various metal oxides used as a supercapacitor electrode material because of its low cost, environmentally friendly, and high theoretical specific capacitance (1370 F g^{-1}).[13,14] Furthermore, MnO_2-based materials are typically applied in neutral aqueous electrolytes, which fulfill the environmental requirements of "green electrolytes" in supercapacitors.[15–17] However, its poor electrical conductivity limits its application. Thus, loading MnO_2 materials on carbon materials, such as carbon nanotubes, carbon fibers, graphene, and graphene aerogel, is essential.[18-24] Jiang et al.[18] designed and synthesised rGO/CNTs/MnO_2 nanocomposites with a high specific capacitance of up to 319 F g^{-1} with enhanced rate capability (222 F g^{-1} even at 60 A g^{-1}) in 1 M Na_2SO_4. Luo et al.[21] proposed an easy method to prepare well-ordered whisker-like MnO_2 arrays with carbon fiber, which had excellent long cycle life property. Wu et al.[22] developed a high-voltage (2.0 V) asymmetric electrochemical capacitor, where graphene served as a negative electrode and MnO_2 nanowire/graphene as a positive electrode in a neutral aqueous Na_2SO_4. Ji et al.[24] anchored MnO_2 on graphene aerogel as the electrode material, which exhibited good electrochemical stability. Huang et al.[25] synthesized MnO_2@C nanosheet array on a titanium foil via hydrothermal method, but through two hydrothermal steps. Zhu et al.[26] incorporated MnO_2 inside the CMK-3 ordered pore channels, which was modified by using 1 M H_2SO_4 for 3 h in order to improve the accessibility of pore channels and surface reactivity. However, the achievement of these composite materials often requires complex or accurate control of the synthesis process.

Thus, we developed a novel method to fabricate mesoporous MnO_2/C composites for the supercapacitor using a one-step hydrothermal approach without any catalysts or templates.

[a]*College of Materials Science and Engineering, Dalian Jiaotong University, Dalian, 116028, P.R. China. E-mail: wanggx1000@126.com*
[b]*Liaoning Provincial Key Laboratory of New Energy Battery, Dalian Jiaotong University, Dalian, 116028, P. R. China. E-mail: hfxu@fuelcell.com.cn*

Unlike conventional approaches, this method not only avoids the subsequent complicated procedure for the removal of the template, but also the hydrothermal process contains self-assemble process of MnO_2 and carbonization of glucose without any active pretreatment, which simplifying the preparation process of the mesoporous MnO_2/C composites. The whisker-like MnO_2 arrayed on carbon sphere surface with a mesoporous structure, a large surface area, and porosity facilitated the rapid transport of electrons and ions in the electrode. An asymmetric supercapacitor with MnO_2/C composites as the positive electrode and active carbon as the negative electrode in 5 M $LiNO_3$ electrolyte indicated high specific capacitance and energy density, as well as good cycling stability with a wide voltage region of 0 to 2.0 V.

Experimental section

Synthesis of samples

All reagents were of analytical grade and were used directly without further purification. Deionized (DI) water was used throughout the experiment. The typical synthesis process of MnO_2/C composites is described as follows: First, 0.1 g glucose was dispersed into 20 mL DI water through ultrasonic vibration for 30 min. Second, 1.35 g manganese sulfate monohydrate ($MnSO_4$•H_2O) was added in the suspension and the mixed solution was stirred by magnetic bar for 6h. Third, 1.82g ammonium persulfate ($(NH_4)_2S_2O_8$) was added with further stirred for a short, after that the mixed solution was transferred to a 50 mL Teflon-lined stainless steel autoclave and treated hydrothermally at 180 °C for 3 h. Finally, products were harvested by centrifugation upon cooling down to room temperature, rinsed several times with DI water and absolute ethanol, and then dried at 80 °C for 12 h.

Material characterization

The crystal structure of the products was characterized by X-ray diffraction (XRD) with a Rigaku D/max UltimaIII using Cu Kα radiation (λ = 1.50405 Å). The morphology and structure of the synthesized materials were investigated using filed emission scanning electron microscopy (FESEM, Hitachi S4300). Specific surface area and pore size distribution (PSD) curves were determined by a Brunauer-Emmett-Teller (BET) measurement (ASAP 2020).

Electrochemical measurement

The electrochemical performance of the MnO_2/C composites and the MnO_2 was evaluated by the three-electrode cell method. The working electrode was prepared by mixing 80 wt% active material, 10 wt% acetylene black, and 10 wt% polyterafluoroethylene (PTFE, 60 wt% dispersion in water). Afterwards, the slurry was spread onto a nickel foam current collector (1 × 1 cm). A platinum wire (1 mm in diameter) and Hg/Hg_2Cl_2 electrode (SCE, saturated KCl, 0.214 V *vs.* NHE at 25 °C) were used as the counter and reference electrodes, respectively. The active carbon electrode was measured within a potential window of -1.0 to 0.0 V, whereas MnO_2 and MnO_2/C spheres were measured within a potential window of 0.0 V to 1.0 V at a scan rate of 10 mV s^{-1}. The asymmetric supercapacitor was measured in a two-electrode system, which contained two slices of an electrode material with the same size. The MnO_2 and MnO_2/C composites in the two electrode system were the positive electrode, and the active carbon (AC) was mixed with 10 wt% acetylene black and 5 wt% PTFE (60 wt% dispersion in water) to fabricate the negative electrode. All other electrochemical characterization was performed using AUTOLAB (ECO CHEMIE, PGSTAT 100) in 5 M $LiNO_3$ aqueous solution as electrolyte at room temperature and normal pressure.

Results and discussion

Fig. 1(a) shows the XRD patterns of the prepared carbon sphere and MnO_2/C composites. The large peaks at 26° and 43° indicated the graphitic character of the carbon sphere,[27] whereas the other three peaks at 2θ = 12.8° (001), 36.8° (111) and 65.7° (311) in the MnO_2/C composite, correspond to the diffraction peaks of the birnessite-type MnO_2 (JCPDS 80-1098).[25] The broadened and weakened peaks of the MnO_2 indicated poor crystallinity in the composite,[28] which was favourable for the supercapacitor.[29] Fig. 1(b) shows the SEM image of bare carbon sphere with diameter of 1 μm and plain surfaces which was glucose treated hydrothermally at 180 °C for 3 h. Figs. 1(c, d) show the images of the MnO_2 and MnO_2/C composites. MnO_2 arrays could be clearly seen from Fig. 2(e,f), in which each sphere was significantly rough-coated with MnO_2 nanowhiskers. This sphere-whisker structure, which was mesoporous and with a high specific surface area, was favourable for improving the main pseudocapacitance of MnO_2 and the electric double-layer (EDL) capacitance of the carbon sphere given that the hydrated ions in the electrolyte are easily accessible to the exterior and interior pore surfaces.[30,31]

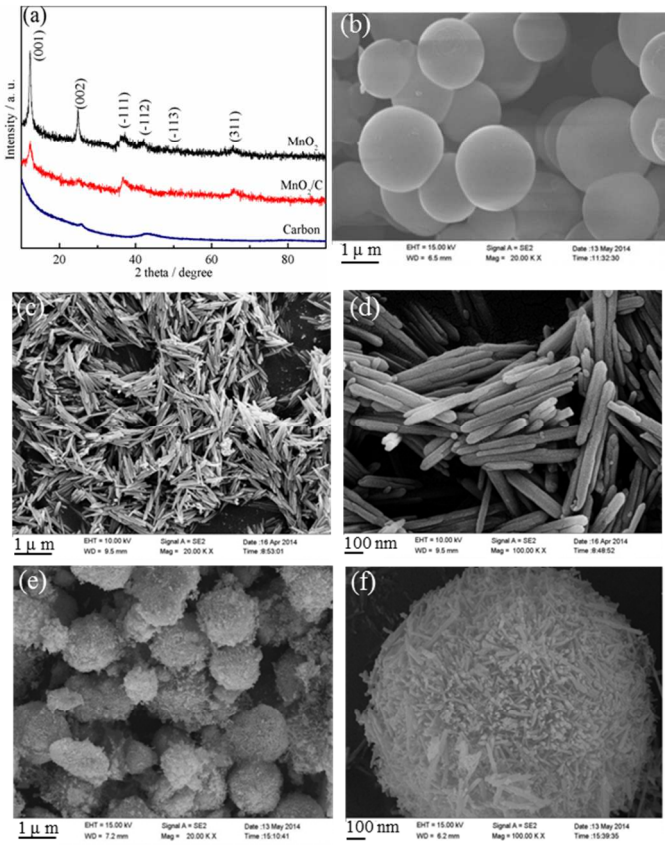

Fig. 1 (a) X-Ray diffraction patterns of samples; SEM images of (b) carbon sphere, (c,d) MnO_2 and (e,f) MnO_2/C composite.

Fig. 2 shows the TEM images of MnO_2/C composite. The carbon sphere had a graphitic structure with a diameter of ~1 μm. When coated with MnO_2, the size of the sphere-whisker structure increased to ~1.5 μm with the length of MnO_2 whisker of 200 nm. Noted that MnO_2 whiskers grown on the carbon sphere, making the composite promising for higher energy storage capacity. HRTEM image further indicated that the interplanar spacing of birnessite-type MnO_2 whisker was ~0.69 nm (Fig. 2b), which was in accordance with the literature.[32,33] The electron diffraction (ED) pattern (Fig. 2(d), inset), taken from a randomly chosen area, showed MnO_2 with a polycrystalline nature.

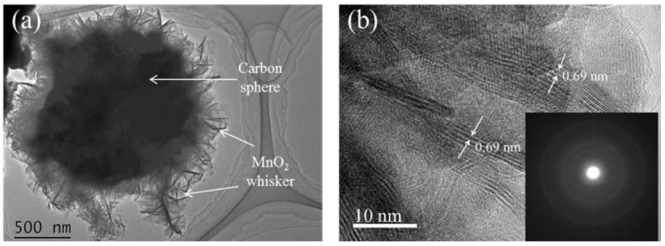

Fig. 2 (a) TEM and (b) HRTEM images of MnO_2/C composite, inset showed the corresponding SAED pattern.

Fig. 3 shows the nitrogen adsorption-desorption isotherm and Barrett-Joyner-Halenda (BJH) pore size distribution curves of the carbon, MnO_2 and MnO_2/C composites. The hysteresis loop in relative pressure (P/P_0) range from 0.45 to 0.90, which might be ascribed to the presence of a mesoporous structure,[34,35] and from 0.9 to 1.0 provided the interpolate space that primarily showed the mesoporous structure in the MnO_2/C composites (Fig. 3(a)). Owing to the adding of the carbon sphere, the surface area of the MnO_2/C composites (142.46 m^2 g^{-1}) was much higher than that of MnO_2 (64.59 m^2 g^{-1}), as well as the BJH pore size distribution curves (Fig. 3(b)), which exhibited the distribution of pore sizes between 3 nm and 4 nm. So the well-fined, pore-size mesoporous structure of MnO_2/C composites facilitated an effective electrolyte diffusion and rapid charge transfer, which can facilitate a high electrochemical performance.[36] Detailed structural parameters are summarized in Table 1.

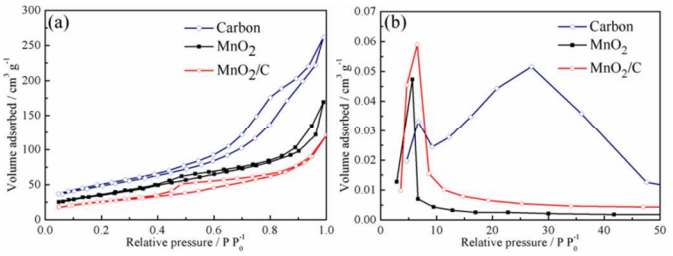

Fig. 3 (a) N_2 adsorption-desorption isotherms and (b) corresponding pore size distribution of the as-prepared carbon, MnO_2 and MnO_2/C composite.

Table 1 Structure and parameters of the carbon, MnO_2 and MnO_2/C composite

Sample	BET area / m^2 g^{-1}	Total pore volume /cm^3 g^{-1}	Average pore size /nm
Carbon	353.82	0.34	26.98
MnO_2	64.59	0.16	3.81
MnO_2/C	142.46	0.27	4.32

Fig. 4 presents the designed formation process to achieve mesoporosity and a high specific surface area for MnO_2/C composites. Glucose was briefly dissolved in DI water, whereas $MnSO_4$ was initially dispersed in glucose solution. $(NH_4)_2S_2O_8$ was then added to the solution, which was treated in hydrothermal reaction to produce the final product after. The following reasons may account for the formation of mesoporous MnO_2/C composites. First, the Mn^{2+} cation was favourable to adsorb at the surface of the carbon sphere with increasing of adding $MnSO_4$ solution and ultrasonic time, which would form a molecular adsorption state. MnO_2 solid deposited on the surface of the carbon sphere as a result of the reaction. Second, the Ostwald ripening process[37] occurred as the hydrothermal reaction further proceeds, in which whisker-like MnO_2 form on the surface carbon sphere because of the "oriented attachment" and "self-assembly" processes,[37] which involved a spontaneous self-organization of the nanowhisker.[38,39] Third, the resulting ions, such as CO_3^{2-} and HCO_3^- inside the carbon sphere during the reaction, which had played an important role in the formation of the pores or pore channels, facilitated forming the large porosity of MnO_2/C composites.[40]

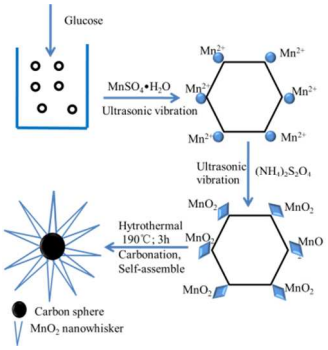

Fig. 4 Schematic illustration a procedure to fabricate MnO_2/C composite.

We performed cyclic voltammograms (CV) of the ECs in a 5 M $LiNO_3$ aqueous solution using a three-electrode system to evaluate the electrochemical properties and quantify the specific capacitance of the as-prepared MnO_2 and MnO_2/C spheres. Fig. 5(a) shows that the CV curves of these electrodes had the nearly ideal rectangular shape, which indicated the efficient charge transfer and the almost ideal capacitive behaviours. Note that no apparent redox peaks were observed at the voltage of 0.0 V to 1.0 V, which due to MnO_2 electrode in mild aqueous electrolyte is a fast, reversible successive multiple surface redox reaction, whose shape is close to that of the EDLC.[41] Based on these results, we could see that the stable voltage window between 0.0 V to 1.0 V was for MnO_2/C composites and between -1.0 V to 0 V was for active carbons with capacitive behaviour, relative to the SCE. Therefore, the operating cell voltage could be extended to about 2.0 V in a mild aqueous solution because of the existing MnO_2 with higher cutoff potential (1.0 V) in the electrode materials, and the active carbon with a lower cutoff potential window (-1.0 V), which were assembled into asymmetric ECs.[42–44] The asymmetric EC was constructed by using MnO_2 and MnO_2/C as the positive electrode and AC as the negative electrode and characterized by using a 5 M $LiNO_3$ solution as electrolyte to evaluate the potential application in EC. Based on charge balance theory, the charge stored by each electrode will follow the relationship $q^+ = q^-$. Accordingly, the mass balancing will follow eqn. (1):[45]

$$m^+ : m^- = (C^- \times \Delta E^-) : (C^+ \times \Delta E^+) \quad (1)$$

Where m, C, and ΔE represent the mass, the specific capacitance, and the potential range for the charge-discharge process of electrode, respectively.

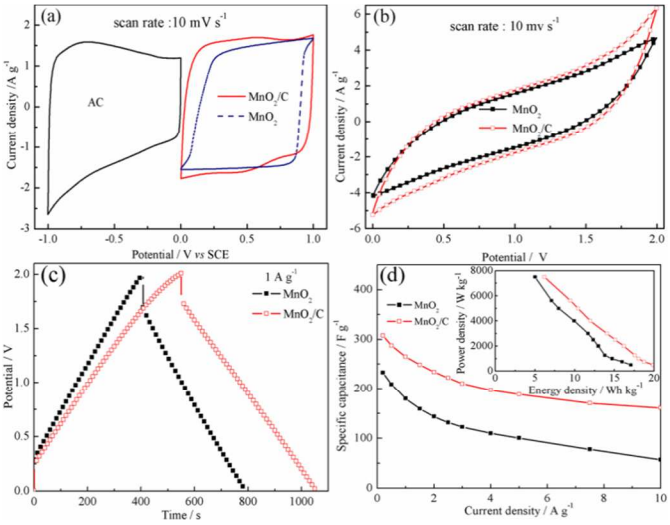

Fig. 5 (a) CV curves of AC and MnO_2/C composite electrodes performed in three-electrode; (b) CV curves of (b) CV curves of MnO_2/C//AC at different scan rates with a wide potential windows of 2.0 V; (c) galvanostatic charge-discharge curves of MnO_2/C//AC at different current densities; (d) Correlation of specific capacitances with discharge currents of MnO_2/C//AC and inset (d) Ragone plots of the power density versus energy density of MnO_2/C//AC.

Fig. 5(b) shows the typical CV curves of MnO_2 and MnO_2/C spheres measured at a scan rate of 10 mV s^{-1}, which exhibited a rectangular-like shape without obvious redox peaks, suggesting that the pseudocapacitive reactions that occurred between the MnO_2 and electrolyte was fast and reversible.[46] The current responses of the MnO_2/C//AC EC was larger than the MnO_2//AC EC, which implied higher specific capacitance value. The excellent specific capacitance of the MnO_2/C//AC EC was mainly attributed to the addition of the carbon sphere. Although the shapes of the CV curves deviated from ideal rectangular shape, the areas surrounded by the CV curves were not significantly influenced by the increasing scan rate, which indicated the desirable fast charge-discharge property of the sample. To further evaluate the electrochemical performance of the MnO_2 and MnO_2/C composites, galvanostatic charge/discharge tests were conducted at a current density of 1 A g^{-1} as shown in Fig. 5(c) between 0 V and 2.0 V. The almost triangular shapes reversed the Faradic reaction for charge storage. Thus, the increased discharge time for MnO_2/C composites suggested a better capacitance performance because of the mesoporous structure and favourable pore connectivity. Furthermore, the specific capacitance (C_A) of the two complete two-electrode system (Fig. 5(d)), as well as the energy and power densities (E_D, P_D) (inset Fig. 5(d)) were calculated on the basis of the galvanostatic charge-discharge result and using the relation provided below:

$$C_A = C/m = (I \times dt) / (dV \times m) \quad (2)$$

$$E_D = CV^2 / 2m \quad (3)$$

$$P_D = IV / 2m \quad (4)$$

Where C is the total measured capacitance of the two-electrode system; I is the constant current used during discharge; dt is the discharge time; dV is the voltage difference during time and m is the mass of the active material on the electrode. A slight decrease in the capacitance of MnO_2/C was observed with increasing current density from 0.5 A g^{-1} to 10 A g^{-1}. This result implied the fast charge transfer of the EC due to the mesoporous structure which reduced the internal resistance of the composite electrode. The MnO_2/C//AC delivered high energy and power densities because of the enhanced specific capacitance and the enlarged working voltage (from 1.0 V to 2.0 V). The energy density reached 19.9 Wh kg^{-1} at a power density of 500 W kg^{-1}, and remained at 6.2 Wh kg^{-1} with a power density of 8000 W kg^{-1}. The high performance of the asymmetric ECs could be ascribe to the following factors: (1) the wide operating cell voltage (2.0 V), in which the cell voltage was extended to 2.0 V resulting in a large increase in energy density; (2) MnO_2/C composites provided a porous structure with mesopores in addition to their high electrical conductivity, superior mechanical properties, and the surface area providing a fast interconnected network for the transport of electrons and ions.[47–49]

The long-term cycling performance of the asymmetric supercapacitor was crucial for practical applications. Fig. 6 shows the capacitance fading over 1000 cycles between a maximum working voltage (2.0 V) for the two samples. The capacitance fading of capacitors with MnO_2/C and MnO_2 were able to retain about 96.6 and 90.1%, respectively. These results suggested the long-term electrochemical stability of the MnO_2/C composites at current density of 1 A g^{-1} for consecutive 1000 cycles, which signified a good mechanical stability of the MnO_2/C composites. The cycling performance at progressively increased current density was recorded in Fig. 6(b) to further understand the stability for MnO_2/C and MnO_2. The mesoporous MnO_2/C composites consistently demonstrated stable capacitance even when suffering from a change of the current delivery. After 300 cycles, a capacitance of 305.3 F g^{-1} could be recovered without any decrease as the current density diminishes to 0.2 A g^{-1} for another 50 cycles. This finding indicated that the MnO_2/C composites had excellent rate performance and cyclability assigned to the unique sphere-whisker structure of MnO_2/C composites (positive electrode), which could improve the stability by effectively preventing the aggregation of carbon sphere and provide a specific surface area with rich mesoporous structure of MnO_2 nanowhisker.

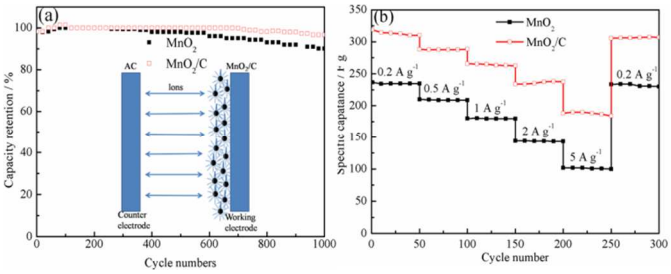

Fig. 6 (a) Capacitance retention at 1 A g^{-1} over 1000 cycles; (b) Charge/discharge capacity at various rates for 350 cycles.

The impedances of MnO_2/C and MnO_2 electrodes were measured at frequencies from 100 kHz to 0.01 Hz to identify the relationship between electrochemical performance and electrode kinetics. Fig. 7 shows that both electrodes exhibited a liner spike at low frequency characterized capacitive behaviour, which demonstrated the common equivalent circuit descriptions of these features: the intercept on the real part at the high-frequency end was ohmic resistance (R_s), including the resistance of intrinsic resistance of substrate, contact resistance at the active material/current collector interface and ionic resistance of electrolyte, and was mainly controlled by the ionic resistance of the electrolyte. The R_s of the two electrodes were almost the same value of 0.8 Ω, because both the electrodes

were tested in 5 M $LiNO_3$ electrolyte; with the size of the semicircular that encompasses the medium-frequency response, was an indication of the charge-transfer resistance (R_{ct}) and a parallel constant phase element (C_d) in the electrode reaction; and the inclined line in the low-frequency region represented the Warburg impedance (Z_w) relative to the electrolyte ions' diffusion/transport throughout the electrode.[50–52] As shown in Fig. 7(a), a major difference was observe on the R_{ct}. MnO_2/C composite electrode indicated a low value at 0.6 Ω and a linear vertical curve, which suggested better capacitive behaviour of the composite electrode compared to that of the MnO_2 electrode (1.5 Ω) in the low frequency region.[49] These results might be attributed to the fast electron transition and the good contact between the current-collector and whisker arrays associated with the sphere-whisker mesoporous structure of the MnO_2/C composites, which confirmed that the MnO_2/C composites was a promising supercapacitor electrode material.

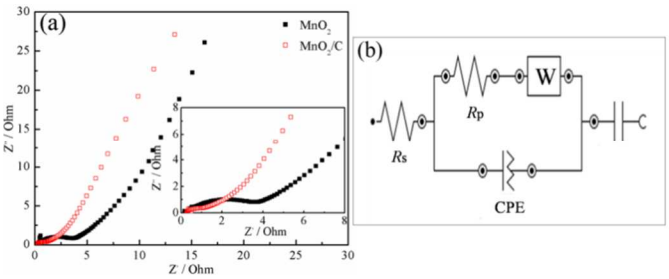

Fig. 7 (a) Nyquist plots of MnO_2/C and MnO_2 electrodes before and after cycles; (b) The electrical equivalent circuit used for fitting impedance spectra.

Conclusions

A simple, low-cost synthesis of nanowhisker MnO_2 anchored to carbon sphere was demonstrated. The mesoporous structure easily forms an efficient conducting network and serves as a favourable buffer in relieving the internal stress that occurs during Faradic processes, further, protecting the electrode from physical damage. Asymmetric EC based on the MnO_2/C composites as positive electrode and AC as negative electrode was assembled in a 5 M $LiNO_3$ aqueous. EC can be utilized in a wide voltage region of 0 V to 2.0 V, which enhanced the specific capacitance at 307.6 F g^{-1} and indicated a good capacitance retention of 96.6% over 1000 cycles. Therefore, the present MnO_2/C nanocomposites can serve as an attractive candidate material for supercapacitor electrodes.

Acknowledgements

This work was supported by the Nation High Technology Research and Development Program of China (863 Program, 2012AA052002) and the National Natural Science Foundation of China (no. 21376034, 21273025)

Notes and references

1 P. Simon and Y. Gogotsi, *Nat. Mater.*, 2008, **7**, 845.
2 H. Jiang, J. Ma and C. Z. Li, *Adv. Mater.*, 2012, **24**, 4197.
3 S. W. Lee, N. Yabuuchi, B. M. Gallant, S. Chen, B. S. Kim, P. T. Hammond and Y. Shao-Horn, *Nat. Nanotechnol.*, 2010, **5**, 551.
4 J. Yan, E. Khoo, A. Sumboja and P. S. Lee, *ACS Nano*, 2010, **4**, 4247.
5 J. R. Miller and P. Simon, *Science*, 2008, **321**, 651.
6 J. W. Lee, T. Ahn, J. H. Kim, J. M. Ko and J. D. Kim, *Electrochimica Acta*, 2011, **56**, 4849.
7 C. Z. Yuan, A. Cao, L. F. Shen, S. D. Yang, L. Hao, X. J. Lu, F. Zhang, L. J. Zhang and X. G. Zhang, *Nanoscale*, 2011, **3**, 529.
8 X. M. Feng, Z. Z. Yan, N. N. Chen, Y. Zhang, Y. W. Ma, X. F. Liu, Q. L. Fan, L. H. Wang and W. Huang, *J. Mater. Chem. A*, 2013, **1**, 12818.
9 W. Chen, R. B. Rakhi, L. Hu, X. Xie, Y. Cui and H. N. Alshareef, *Nano Lett.*, 2011, **11**, 5165.
10 Y. Huang, J. Liang and Y. Chen, *Small*, 2012, **8**, 1805.
11 J. Yan, E. Khoo, A. Sumboja and P. S. Lee, *ACS Nano*, 2010, **4**, 4247.
12 B. G. Choi, M. Yang, W. H. Hong, J. W. Choi and Y. S. Huh, *ACS Nano*, 2012, **6**, 4020.
13 H. Jiang, T. Zhao, J. Ma, C. Y. Yan and C. Z. Li, *Chem. Commun.*, 2011, **47**, 1264.
14 H. Jiang, T. Zhao, C. Y. Yan, J. Ma and C. Z. Li, *Nanoscale*, 2010, **2**, 2195.
15 W. Tang, Y. Y. Yang, F. X. Wang, L. L. Liu, Y. P. Wu and K. Zhu, *Nano Lett.*, 2013, **13**, 2036.
16 Q. T. Qu, P. Zhang, B. Wang, Y. H. Chen, S. Tian, Y. P. Wu and R. Holze, *J. Phys. Chem. C*, 2009, **113**, 14020.
17 X. M. Feng, N. N. Chen, Y. Zhang, Z. Z. Yan, X. F. Liu, Y. W. Ma, Q. M. Shen, L. H. Wang and W. Huang, *J. Mater. Chem. A*, 2014, **2**, 9178.
18 H. Jiang, Y. H. Dai, Y. J. Hu, W. N. Chen, C. Z. Li, *ACS Sustainable Chem. Eng.*, 2014, **2**, 70.
19 Y. Hou, Y. W. Cheng, T. Hobson and J. Liu, *Nano Lett.*, 2010, **10**, 2727.
20 H. Zhang, G. P. Gao, Z. Y. Wang, Y. S. Yang, Z. J. Shi and Z. N. Gu, *Nano Lett.*, 2008, **8**, 2664.
21 Y. S. Luo, J. Jiang, W. W. Zhou, H. P. Huang, J. S. Luo, X. Y. Qi, H. Zhang, D. Y. W. Yu, C. M. Li, Ting Yu, *J. Mater. Chem.*, 2012, **22**, 8634.
22 Z. S. Wu, W. C. Ren, D. W. Wang, F. Li, B. L. Liu and H. M. Cheng, *ACS Nano*, 2010, **4**, 5835.
23 L. L. Peng, X. Peng, B. R. Liu, C. Z. Wu, Y. Xie, G. H. Yu, *Nano Lett.*, 2013, **13**, 2151.
24 C. C. Ji, M. W. Xu, S. J. Bao, Z. J. Lu, C. J. Cai, H. Chai, R. Y. Wang, F. Yang and H. Wei, *New J. Chem.*, 2013, **37**, 4199.
25 Y. Huang, Y. Y. Li, Z. Q. Hu, G. M. Wei, J. L. Guo and J. P. Liu, *J. Mater. Chem. A*, 2013, **1**, 9809.
26 S. M. Zhu, H. S. Zhou, M. Hibino and I. Honam and M. Ichinara, *Adv. Funct. Mater.*, 2005, **15**, 381.
27 M. X. Liu, L. H. Gan, W. Xiong, Z. J. Xu, D. Z. Zhu and L. W. Chen, *J. Mater. Chem. A*, 2014, **2**, 2555.
28 J. X. Zhu, W. H. Shi, X. Ni, X. H. Rui, H. T. Tan, X. H. Lu, H. H. Hng, J. Ma and Q. Y. Yan, *ACS Appl. Mater. Interfaces*, 2012, **4**, 26.

29 S. J. Bao, B. L. He, Y. Y. Liang, W. J. Zhou and H. L. Li, *Mater. Sci. Eng.*, 2005, **397**, 305.
30 M. B. Zheng, J. Cao, S. T. Liao, J. S. Liu, H. Q. Chen, Y. Zhao, W. J. Dai, G. B. Ji, M. Cao and J. Tao, *J. Phys. Chem. C*, 2009, **113**, 3887.
31 J. P. Ma, Q. L. Cheng, V. Pavlinek, P. Saha, C. Z. Li, *New J. Chem.*, 2013, **37**, 722.
32 T. T. Truong, Y. Liu, Y. Ren, L. Trahey and Y. Sun, *ACS Nano*, 2012, **6**, 1855.
33 Y. Wang, S. F. Yu, C. Y. Sun, T. J. Zhu and H. Y. Yang, *J. Mater. Chem.*, 2012, **22**, 17584.
34 J. Y. Baek, H. W. Ha, I. Y. Kim, S. J. Huang, *J. Phys. Chem. C*, 2009, **113**, 17392.
35 H. Jiang, L. P. Yang, C. Z. Li, C. Y. Yan, P. S. Lee and J. Ma, *Energy Environ. Sci.*, 2011, **4**, 1813.
36 L. B. Kong, M. Liu, J. W. Lang, Y. C. Luo and L. Kang, *J. Electrochem. Soc.*, 2009, **156**, A10000.
37 T. Brouss, P. L. Taberna, O. Crosnier, R. Dugas, P. Guillemet, Y. Scudeller, Y. Zhou, F. Favier, D. Belanger and P. Simon, *J. Power Sources*, 2007, **173**, 633-641.
38 M. S. Hong, S. H. Lee and S. W. Kim, *Electrochem.Solid-state Lett.*, 2002, **5**, A227.
39 D. W. Wang, F. Li, M. Liu, G. Q. Lu and H. M. Cheng, *Angew. Chem., Int. Ed.*, 2008, **47**, 373.
40 P. H. Yang, Y. Z. Li, Z. Y. Lin, Y. Ding, S. Yue, C. P. Wang, X. Cai, S. Z. Tan and W. J. Mai, *J. Mater. Chem. A*, 2014, **2**, 595.
41 P. Simon and Y. Gogotsi, *Nature Materials*, 2008, **7**, 845.
42 S. S. Wu, W. F. Chen and L. F. Yan, *J. Mater. Chem. A*, 2014, **2**, 2765.
43 J. B. Fei, Y. Cui, X. H. Yan, W. Qi, Y. Yang, K. W. Wang, Q. He and J. B. Li, *Adv. Mater.*, 2008, **20**, 452.
44 X. Zhao, C. Johnston, A. Crossley and P. S. Grant, *J. Mater. Chem.*, 2010, **20**, 7637.
45 S. J. Bao, C. M. Li, C. X. Guo and Y. Qiao, *J. Power Sources*, 2008, **180**, 676.
46 K. S. Novoselov, A. K. Geim, S. V. Morozov, D. Jiang, Y. Zhang, S. V. Duboonos, L. V. Grigorieva and A. A. Firsov, *Science*, 2004, **306**, 666.
47 M. B. Sassin, C. N. Chervin, D. R. Rolison and J. W. Long, *Acc. Chem. Res.*, 2013, **46**, 1062.
48 A. B. Yuan, X. L. Wang, Y. Q. Wang and J. Hu, *Electrochim. Acta*, 2009, **54**, 1021.
49 K. B. Xu, W. Y. Li, Q. Liu, B. Li, X. J. Liu, L. An, Z. G. Chen, R. J. Zou and J. Q. Hu, *J. Mater. Chem. A*, 2014, **2**, 4795.
50 H. Xia, M. O. Lai, L. Lu, *J. Mater. Chem.*, 2010, **20**, 6896.
51 W. Xiao, H. Xia, J. Y. H. Fuh and L. Lu, *J. Electrochem. Soc.*, 2009, **156**, A627.
52 X. G. Wang, L. Gu and C. L. Cui, *ACS Nano*, 2013, **7**, 5430.

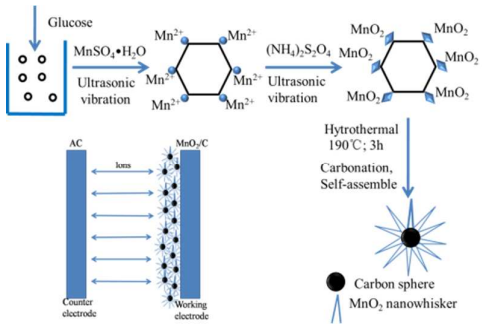

The mesoporous MnO_2/C composites were simply synthesised using one-step hydrothermal approach that not only without any catalysts or templates, but also the carbon from carbonization of glucose without any active pretreatment.